WearaCob: A Unified Bidirectional Framework for Adaptive Synergy Between Wearable and Collaborative Robotics

Sandro Ferrari[1], Ivan Terrile[2], Francesco Missiroli[1], Federico Masiero[1], Maura Casadio[2], and Lorenzo Masia[1]

***Abstract*—The advent of Human-Robot Collaboration has redefined industrial automation by reestablishing the human operator as a central agent in shared workspaces. While collaborative robots (cobots) enable safe and intuitive interaction, the parallel rise of wearable assistive devices, such as occupational exoskeletons, addresses growing concerns over operator fatigue and musculoskeletal strain. This paper presents *WearaCob*, an integrated system combining a vision-enhanced bimanual elbow soft exoskeleton with an industrial cobot to enable synergistic, user-adaptive collaboration. The system fosters bidirectional adaptation: the exoskeleton modulates its assistance in real time based on external load data communicated by the cobot, while the cobot tailors object handovers using user localization and anthropometric information from the exoskeleton. In a simulated logistics scenario, *WearaCob* demonstrated precise and robust handover execution, while maintaining consistent muscular effort across increasing loads, achieving up to 65% reduction in biceps activation compared to the exoskeleton alone without bidirectional communication with the cobot. These findings highlight *WearaCob*'s potential to enhance the efficiency, safety, and adaptability of human-robot collaboration, marking a step toward a new era of assistive industrial automation.**

***Index Terms*—Human-Robot Interaction, Wearable Robotics, Collaborative Robotics, Adaptive Assistance Systems, Real-Time Communication in Robotics, Systems Integration.**

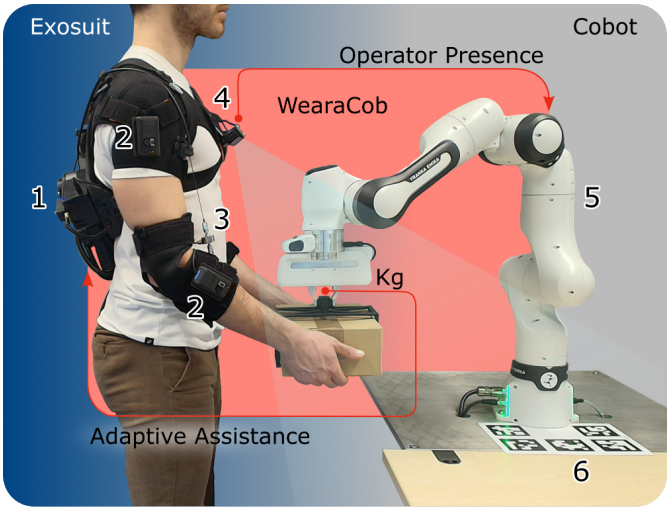

Fig. 1. The system emulates a logistics workcell. An operator wearing a bimanual tendon-driven elbow soft exoskeleton receives a payload from a collaborative robotic arm. The soft exoskeleton includes: (1) back protector housing two electromechanical actuators, vision module control board, and battery; (2) Inertial Measurement Unit; (3) load cell; and (4) RGB camera. Also shown are (5) the collaborative robot and (6) fiducial markers.

I. Introduction

RECENT advancements in Smart Industry have transformed manufacturing, logistics, and maintenance by embedding humans as central agents in flexible and adaptive work environments [1], [2]. This transformation arises because full automation is neither economically viable nor desirable, whereas human adaptability and cognitive abilities still surpass those of machines [3]. This human-centric automation revolution [4], [5] places a strong emphasis on the study of human-robot collaboration (HRC) [3], [6], [7], which has given rise to collaborative and wearable robotic technologies [3], [8], [9].

Collaborative robots (cobots) emerged to remove traditional barriers promoting shared spaces with human operators, and have recently demonstrated strong potential in adapting task execution to human presence and dynamics [10], [11], [12]. Prior HRC studies have optimized object handover during heavy object handling through control frameworks and task-specific optimization [13], [14], [15]. While these methods reduced effort and improved posture, they offered no assistance beyond the robot workspace, leaving operators unsupported during the remaining manual phases of the task and thus at continued risk of work-related musculoskeletal disorders (WMSDs). Since a cobot interacts solely through physical contact, richer human–robot interaction requires additional sensing, either in the environment or on the operator.

In parallel, occupational exoskeletons have been developed to mitigate operator fatigue and WMSDs, demonstrating clear benefits in lowering joint stress and muscle strain, especially during repetitive lifting and material handling tasks [16], [17], [18]. However, their effectiveness in real-world deployments is often constrained by limited adaptability. Indeed, most systems provide constant or predefined assistance [16], [19], without accounting for variations in external load, user posture, or task context. Emerging approaches to provide exoskeletons with adaptive assistance include embedding biosignals [20], [21] or artificial vision [22], [23] in the control loop. While EMG-based approaches provide modulated assistance via muscle state estimation, they are often impractical in industrial scenarios due to sensor placement, calibration requirements, and robustness issues [19], [24]. In contrast, artificial vision avoids the issue of obtrusiveness often associated with skin-mounted sensors, providing insights into the user's interaction with the

Manuscript received: October, 7, 2025; Revised December, 11, 2025; Accepted February, 7, 2026.

This paper was recommended for publication by Editor Ki-Uk Kyung upon evaluation of the Associate Editor and Reviewers' comments.

[1]: S. Ferrari, F. Missiroli, F. Masiero, and L. Masia are with the Technical University of Munich and Munich Institute of Robotics and Machine Intelligence, Friedrich-Ludwig-Bauer-Straße 3, Garching bei München, Germany.

[2]: I. Terrile and M. Casadio are with the Department of Informatics, Bioengineering, Robotics and Systems Engineering, University of Genoa, Italy.

Corresponding author: Lorenzo Masia (lorenzo.masia@tum.de).

Digital Object Identifier (DOI): see top of this page.

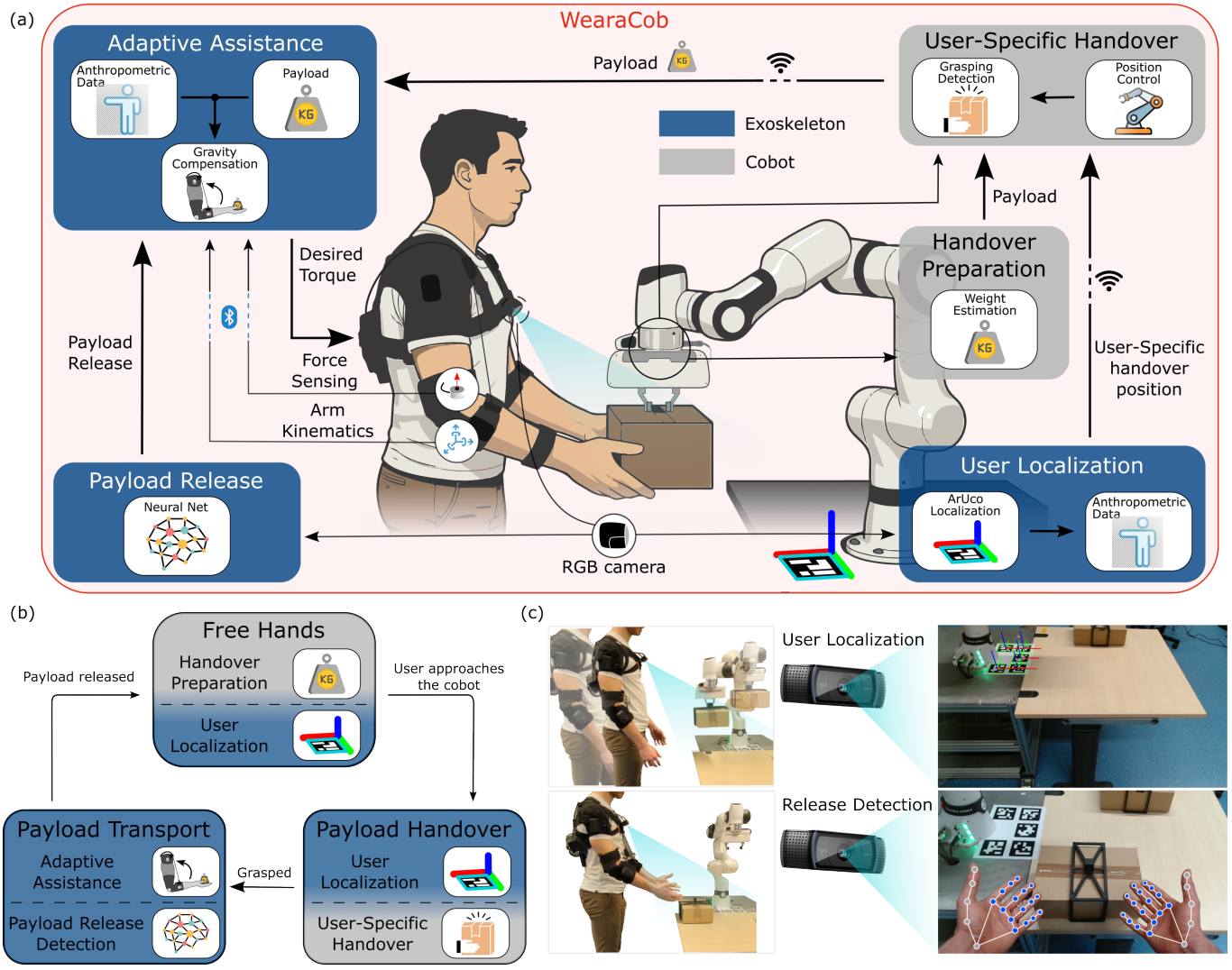

Fig. 2. (a) Diagram of the Shared Control Framework illustrating system information flow. The framework integrates a vision-equipped exoskeleton with a cobot. **Handover Preparation**: the cobot measures the payload's weight and awaits the operator's approach. **User Localization**: the vision module localizes the operator relative to the cobot's reference system and, combined with anthropometric data, informs the cobot of an optimal handover pose. **User-Specific Handover**: as the operator approaches, the cobot places the payload in a personalized position for the user based on the location and anthropometry. Upon detecting grasp, the cobot hands over the payload and communicates the weight information to the exoskeleton controller. **Adaptive Assistance**: the exoskeleton adapts assistance based on the communicated weight. **Payload Release Detection**: a neural network within the vision module detects when the user's hands are free, disabling supplementary assistance. (b) State machine of the Shared Control Framework, orchestrating sequential control logic, starting from the **Free Hands** state. (c) Computer Vision Module presentation. Top row, **User Localization**: left shows the operator approaching the cobot; right displays the chest-mounted camera view with overlaid ArUco marker frames. Bottom row, **Payload Release Detection**: left captures the moment after the operator releases the payload; right shows hand landmarks identified by the neural network, confirming hands-free status.

environment. However, such information is not always fully obtainable (e.g., when handling closed containers).

When examined independently, neither cobots nor exoskeletons can comprehensively address the challenge of assisting human operators across entire tasks: cobots are confined to offering support within their workspace boundaries, whereas exoskeletons exhibit limited capacity to modulate assistance in response to task-specific contexts. Since cobots and exoskeletons share goals but have limitations when operating in isolation, their integration offers new opportunities for industry. A first attempt to integrate these two technologies was recently proposed to address cooperative tasks [25]. In that work, an online optimization strategy is used to plan the trajectory of a cobot holding a box so as to redistribute task-induced torques experienced by a user spray-painting the object toward joints supported by a wearable exoskeleton.

Here, we present *WearaCob*, a system that integrates wearable robots with collaborative robots to enable real-time context-aware assistance modulation and enriched physical human–robot interaction during object handover. Within this framework, an exoskeleton equipped with an onboard camera and informed with user anthropometric data enables real-time localization in the cobot workspace and user-specific object handover. Conversely, the cobot provides real-time measurements of external payloads, which are used to dynamically adapt the assistance provided by the exoskeleton.

We assessed the system in a simulated logistics scenario where a cobot delivered variable payloads for lifting by an

operator wearing a bimanual soft exoskeleton. The system was evaluated by measuring the precision and adaptability of user-specific handover, as well as the reduction in muscular activation experienced by the operator. The main contributions of this study are: (i) conceptualization and implementation of a novel unified framework enabling bidirectional communication between cobots and exoskeletons for adaptive assistance and user-specific handover; (ii) experimental validation in a logistics scenario, demonstrating improvements in handover precision and operator muscle load reduction. Our results show that *WearaCob* enables effective, real-time assistance modulation and advances human–cobot interaction, marking a step toward truly human-centered industrial environments.

II. System Design

WearaCob integrates a soft exoskeleton equipped with a vision module and a cobot (Fig. 1).

The cobot is a Franka Research 3 (Franka Robotics GmbH, Munich, Germany) [26], which measures external forces and cooperates with the human operator in shared workspaces.

The assistive device consists of a bimanual soft exoskeleton designed to provide elbow flexion assistance, counteracting gravitational forces, thereby reducing biceps muscular activation. The utilized exoskeleton is the evolution of a previous work [22]. Each arm is actuated independently by a tendon-driven system mounted on the wearer's back. The system generates tensile forces that are transmitted through a Bowden cable running from the upper arm to the forearm, producing an assistive torque to support elbow flexion against gravity. Elbow extension is not actively assisted, as gravitational forces already act in favor of the movement. The actuation systems implement a gravity compensation strategy based on admittance control using kinematic data, which are acquired from two independent sensing modules, each including an Inertial Measurement Unit (IMU): one attached to the upper arm and the other to the forearm. The forearm sensing module also comprises a load cell to measure the interaction force between the tendon and the user's limb. The exoskeleton control algorithm is implemented in MATLAB/Simulink and deployed on a microcontroller operating at 300 Hz.

The exoskeleton is equipped with a vision module that localizes the user with respect to the robot's reference system and detects the instant at which the user releases the payload using a convolutional neural network. The hardware setup includes an AI computing unit, the NVIDIA Jetson Nano (NVIDIA, Santa Clara, CA, USA), mounted on the user's back, and an RGB camera (C920s, Logitech, Newark, CA, USA) mounted on the user's chest. Moreover, the AI computing unit is responsible for managing communication between the exoskeleton and the collaborative robot (via Wi-Fi).

III. Shared Controller Framework

We propose a shared control framework integrating our exoskeleton with a collaborative robot in a logistics-inspired scenario, Fig. 2(a). The system pursues two objectives: (i) tailoring robot behavior to the operator's anthropometry and movements, and (ii) adaptively modulating exoskeleton assistance in real time. As depicted in Fig. 2(b), the interaction between the cobot, exoskeleton, and vision module is structured as a finite-state machine with three states: Free Hands, Payload Handover, and Payload Transport. Transitions are triggered by user approach (User Localization), payload grasp (Anthropometric User-Specific Handover), and payload release (Payload Release Detection).

In the Handover Preparation process, prior to transferring the payload to the user, the cobot estimates the payload's weight from joint torques under quasi-static conditions:

$$\mathbf{F}_{\text{payload}} = (\mathbf{J}^T)^\dagger \left(\boldsymbol{\tau} - \mathbf{g}(\mathbf{q})\right), \tag{1}$$

where $\mathbf{J}$ is the Jacobian, $\boldsymbol{\tau}$ the measured joint torques, and $\mathbf{g}(\mathbf{q})$ the gravitational forces. With a vertical gripper, only the z-component is considered, yielding: $m_{\text{payload}} = \mathbf{F}_{\text{payload},z}/g$. The cobot then moves to a central standby pose waiting for the user (Free Hands state, Fig. 2b). In parallel, during the User Localization process, the user is localized using a chest-mounted camera on the exoskeleton that detects ArUco markers in the cobot's workspace [27] (Free Hands state, Fig. 2b,c). The handover location is determined from the user's height H_u and the desired elbow angle θ_{des}. The angles θ_e and θ_{des} are defined with respect to the fully extended arm configuration ($\theta_e = 0°$) and increase with elbow flexion.

The horizontal displacement of the payload along the progression axis is given by $d_{\text{pd}} = x_{h,\text{CoM}} \sin(\theta_{\text{des}})$, where $x_{h,\text{CoM}}$ represents the distance from the elbow to the hand's center of mass, computed as $x_{h,\text{CoM}} = 0.201\, H_u$, based on anthropometric tables [28]. The hand's center of mass is chosen to approximate the user's grip point on the payload.

The corresponding vertical placement is expressed as $h_e - x_{h,\text{CoM}} \cos(\theta_{\text{des}})$, where $h_e = 0.630\, H_u$, denotes the user's elbow height from the ground.

While the payload height h_{sh} is expressed in the world reference frame, the horizontal distance d_{pd} must be transformed from the camera to the robot reference frame. For each frame, the poses of all n_a ArUco markers detected within the camera's field of view are inverted, mapped into a common reference frame, and averaged:

$$\mathbf{H}_C^A = \frac{1}{n_a} \sum_{i=1}^{n_a} \mathbf{H}_{A_i}^A \mathbf{H}_C^{A_i}, \tag{2}$$

yielding the camera pose relative to the marker frame. The complete transformation expressing the target pose for payload placement in the ArUco markers' reference frame, $\mathbf{H}_{\text{sh}}^A$, for the user-specific handover is defined as the homogeneous matrix, corresponding to a translation of d_{pd} on the progression axis applied to $\mathbf{H}_C^A$.

The resulting user-specific transformation is transmitted to the cobot controller to guide handover at 19 fps (state Payload Handover, Fig. 2b).

The user localization guides the cobot in the Anthropometric User-Specific Handover process. The cobot maps the user-specific pose $\mathbf{H}_{\text{sh}}^A$ from the ArUco marker frame to its own reference frame using the calibrated transformation $\mathbf{H}_A^R$,

obtained through end-effector tip calibration. The complete user-specific handover pose is expressed as

$$\mathbf{H}_{sh}^{R} = \mathbf{H}_{A}^{R}\mathbf{H}_{sh}^{A}. \tag{3}$$

When the operator grasps the payload and the end-effector force exceeds a predefined threshold, the system transitions to the Payload Transport state (Fig. 2b) and the cobot transmits payload mass and grasp confirmation to the exoskeleton.

This communication influences the online soft exoskeleton Adaptive Assistance process. The soft exoskeleton computes desired elbow torque using a biomechanical arm model [24], [9] extended to also compensate for the manipulated payload:

$$\tau_{\text{des}} = (m_f x_{f,\text{CoM}} + m_{\text{payload}} x_{h,\text{CoM}}) g \sin\theta_e + \ddot{\theta}_e (x_{f,\text{CoM}}^2 m_f + x_{h,\text{CoM}}^2 m_{\text{payload}}), \tag{4}$$

with forearm-hand mass $m_f = 0.022\, M_u$ (user's mass), CoM distances $x_{f,\text{CoM}} = 0.099\, H_u$ and $x_{h,\text{CoM}} = 0.201\, H_u$, elbow angle θ_e [29], and gravitational acceleration $g = 9.81\,\text{m/s}^2$. Coriolis terms are neglected due to low velocities [9].

The exoskeleton actuation control is based on a PID control on the torque error. Interaction torque τ_i calculated from cable tension is compared to τ_{des}:

$$e_r = \tau_{\text{des}} - \tau_i. \tag{5}$$

A PID controller generates the desired motor angular velocity:

$$Y(s) = \frac{\omega_{\text{des}}}{e_r} = \frac{K_p + K_i s^{-1}}{1 + K_d s}, \tag{6}$$

with empirically tuned gains K_p, K_i, K_d.

Finally, after the handover, the Payload Release Detection process is performed. Payload release is detected during Payload Transport using an algorithm based on MediaPipe [31], optimized for real-time execution on a Jetson Nano (28 fps). Release is recognized when fingertips or knuckles reappear, triggering a transition to the Free Hands state and signaling the exoskeleton to cease external load compensation, Fig. 2(c).

All calibration procedures, for User-Specific Handover and Adaptive Assistance, are performed offline without tuning other than user-specific anthropometric measurements.

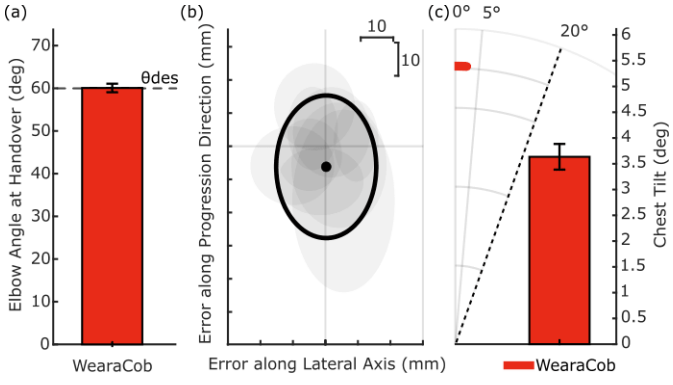

Fig. 3. User-Specific Handover. (a) Bar plot showing mean±SE of the users' elbow angle at handover (θ_{des} denotes target angle). (b) Positioning error of the payload relative to the intended handover location. Each ellipsoid represents mean and standard deviation along the Progression and Lateral directions for a participant; black-bordered ellipsoid indicates the mean and standard deviation across all subjects. (c) Mean±SE of the users' chest inclination at handover, compared to the safety threshold of 20°.

IV. Experiment

Ten healthy participants (eight males; 71.8 ± 9.6 kg, 176.9 ± 5.7 cm, 28.2 ± 4.5 years) took part in the study after providing informed consent in accordance with the Declaration of Helsinki. The protocol was approved by the Institutional Review Board of the Academic Institution (S-311/2020).

The experimental protocol replicated a logistics scenario in which participants received three visually indistinguishable payloads (LW $= 0.8$ kg, MW $= 1.6$ kg, and HW $= 2.4$ kg) from a collaborative robot and subsequently relocated them. Three experimental conditions were tested: *Cob*, where the human–robot interaction was limited to handover without exoskeleton assistance; *Weara*, where the exoskeleton provided constant support based solely on its own sensors; and *Weara-Cob*, where the exoskeleton and robot exchanged information on user location and load, enabling real-time adaptive assistance. The exoskeleton and user-specific handover strategy were applied in all conditions, with $\theta_{\text{des}} = 60°$. This angle was selected based on preliminary experimental trials.

Each trial consisted of four phases: approaching the robot from varying directions, user-specific handover with a symmetric grasp and horizontal payload orientation, manipulation, and final placement. During manipulation, participants lifted the payload to 90° elbow flexion over three seconds, held the posture for five seconds, and lowered it over three seconds, all paced by auditory cues generated and temporized by the cobot controller. The 90° holding posture was chosen to maximize effort, ensuring standardized duration, and facilitating consistent EMG analysis. Familiarization trials were conducted prior to data collection. Each participant completed 54 trials (six per payload weight, for all three conditions) within a single session, with randomized condition order and 30-minute rest periods between the conditions to prevent fatigue.

Data acquisition included kinematics from IMUs (upper arm, forearm, and chest), load cell data measuring tendon tension, vision recording from the exoskeleton camera, and muscular effort from EMG signals recorded at 1 kHz (Delsys Trigno IM) from the right biceps and triceps brachii following SENIAM guidelines [32]. Maximum voluntary contraction (MVC) tests were conducted to normalize EMG activity, enabling inter-subject comparison; one participant was excluded from the triceps analysis due to electrode misplacement. All signals were synchronously recorded for offline processing.

V. Data Analysis

To investigate user-specific handover, elbow angles were measured with IMUs on the arm, filtered with a 4th-order Butterworth filter (6 Hz), and smoothed with a 0.1 s moving average. Angles were averaged over a 0.2 s window centered on the grasp event. Payload placement accuracy was measured via ArUco markers, considering progression and lateral axes. Trunk inclination was collected via a chest-mounted IMU and averaged over 5 s before and after handover.

To assess the effect of adaptive assistance, EMG signals were band-pass filtered (15–450 Hz), rectified, and low-pass filtered (6 Hz). Envelopes were normalized to MVC, and RMS values were extracted during lifting, holding, and lowering.

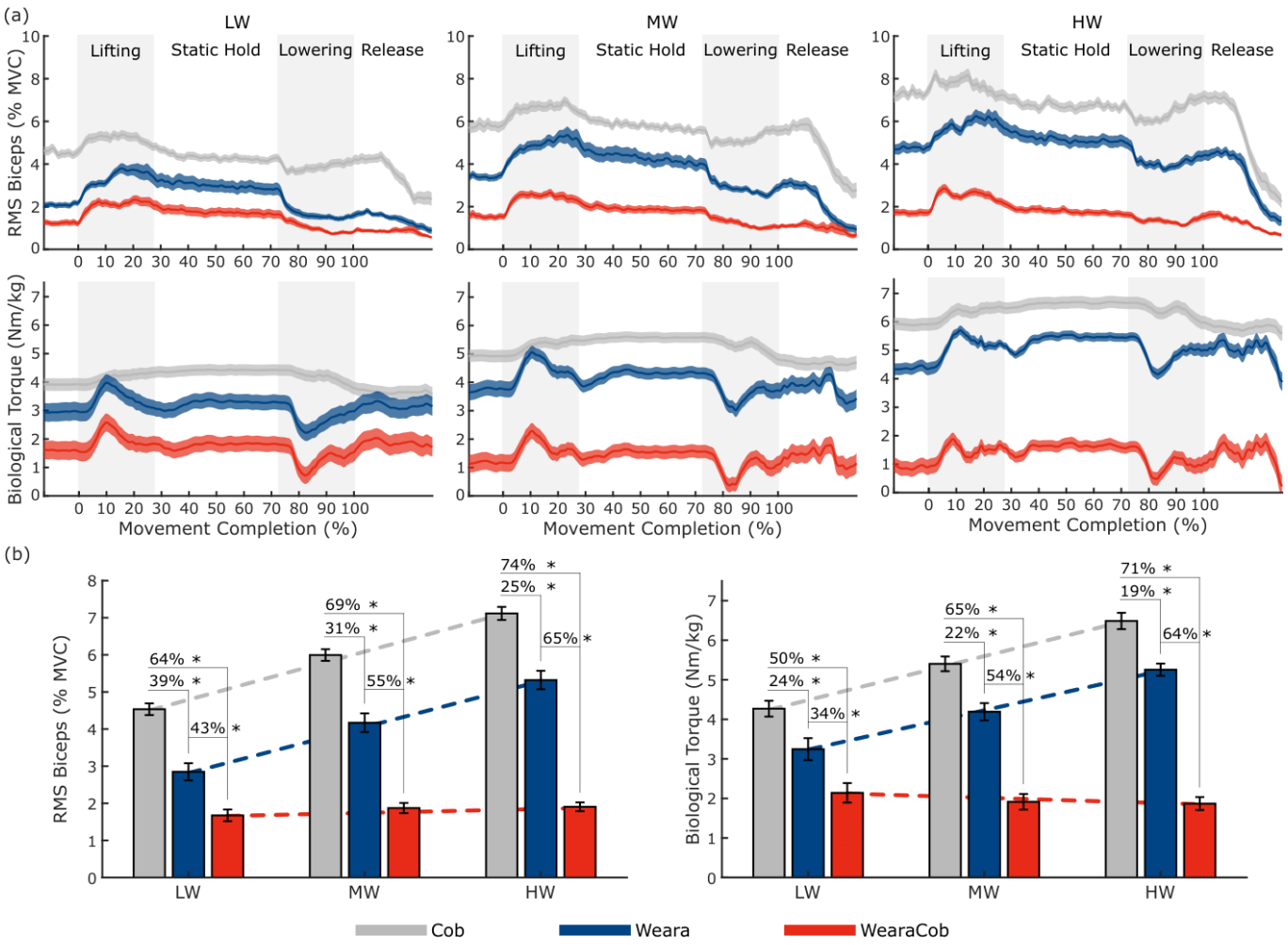

Fig. 4. Muscular Activation and Biological Torque. In all plots, solid lines indicate the mean, and shaded areas represent the standard error across participants. Data are normalized over the movement duration and expressed as a percentage. (a) First row and (b) first bar plot: biceps activation under different external loads (LW, MW, HW). In the *Weara* condition, activation follows a trend similar to *Cob*, with a consistent reduction, while in the *WearaCob* condition, activation remains largely unchanged. (a) Second row and (b) second bar plot: biological torque, which mirrors the trend in biceps activation, as expected, since torque is proportional to biceps activity and is reduced due to the assistive torque provided by the soft exoskeleton. * $p_B < 0.05$.

Biological torque was obtained by subtracting interaction torque (see Section III) from total torque estimated via elbow inverse dynamics (pendulum model) and smoothed with a 0.1 s window. From arm IMUs, we derived elbow angles, angular velocities, start/plateau angles, overshoots, and SPARC [30].

In all the analyses, data normality was assessed with Shapiro–Wilk and variance homogeneity with Levene's test. If valid, repeated-measures ANOVA ($p_A < 0.05$) was applied; otherwise, Kruskal–Wallis ($p_{KW} < 0.05$) was used. Post-hoc pairwise comparisons employed Bonferroni correction ($p_B < 0.0167$). All analyses were performed in MATLAB.

VI. Results

Elbow angle at grasp (Fig. 3a) was $60.46 \pm 1.00°$, closely matching the $60°$ target ($0.46 \pm 1.00°$ error). Payload placement accuracy yielded mean errors of 0.23 ± 15.40 mm laterally and -6.19 ± 21.51 mm along progression (Fig. 3b). Trunk inclination was $3.64 \pm 0.27°$ (Fig. 3c), remaining well below the $20°$ safety threshold [33].

Average profiles of biceps muscular activation (Fig. 4a, upper panels) and biological torques (Fig. 4a, bottom panels) during task execution are reported for all weights and experiment conditions. Both *Weara* and *WearaCob* conditions demonstrated significant muscular reductions in *biceps brachii* averaged RMS across all load conditions with respect to the *Cob* condition, in which no assistance was provided by the exoskeleton (Fig. 4b, left panel). In the *Weara* condition muscular activation decreased up to 39% with respect to the *Cob* condition, reducing the RMS value from $4.55 \pm 0.16\%$ to $2.79 \pm 0.23\%$ ($p_B < 0.001$ for the low-weight condition). In the *WearaCob* condition, muscular activation decreased up to 74% with respect to the *Cob* condition, reducing the RMS value from $7.14 \pm 0.18\%$ to $1.85 \pm 0.11\%$ ($p_B < 0.001$, for the heavy-weight condition). In addition, the *WearaCob* condition demonstrated significant muscular reductions with respect to the *Weara* condition regardless of the payload weight (up to 65%, for the heavy-weight condition, $p_B < 0.001$).

RMS biceps activation reduction from *Cob* to *Weara* was approximately constant ($\approx$ 1.83). In contrast, *WearaCob*

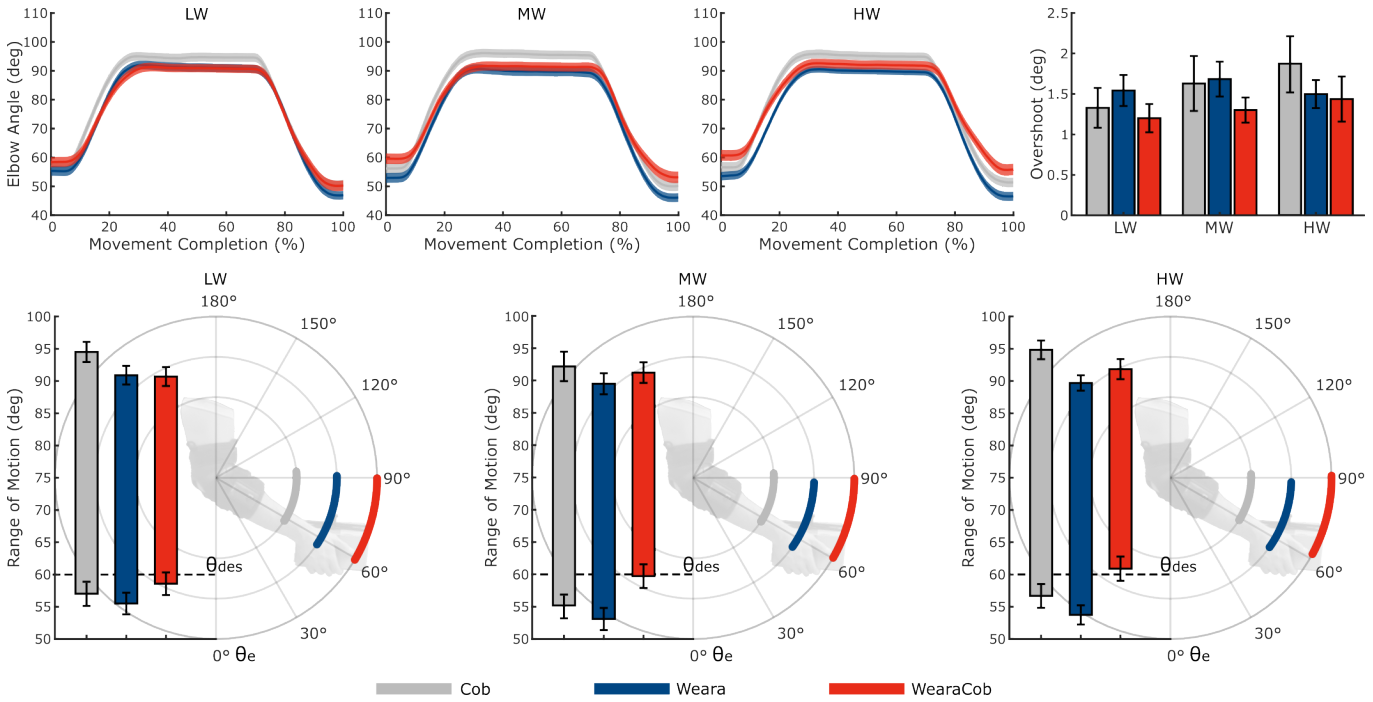

Fig. 5. Elbow Kinematics. This panel shows the elbow trajectory kinematics recorded during the experimental task, including elbow angle profiles, initial angles, plateaus, and overshoots. Data are presented as mean values with standard error across participants. The trajectories are compared across three experimental conditions (*Cob*, *Weara*, *WearaCob*) and three external load levels (LW, MW, HW). Results indicate that neither the experimental condition nor the external load significantly influenced the executed trajectories.

showed no significant differences across payloads (LW–MW: $p_B = 0.04$, LW–HW: $p_B = 0.23$, MW–HW: $p_B = 1$), indicating weight-informed assistance. Similar considerations regarding the average values of the biological torque can be drawn (Fig. 4b, right panel), confirming the modulation of exoskeleton assistance and aligning with the EMG analysis.

The analysis of triceps activation and kinematics data revealed that the system did not impair participants' movements, as reported in Fig. 5, 6. Indeed, we found no significant changes in *triceps brachii* EMG activity ($p_A = 0.22$), starting elbow angles (LW–MW: $p_B = 1$, LW–HW: $p_B = 0.03$, MW–HW: $p_B = 0.03$), plateau angles ($p_A = 0.60$), overshoots ($p_A = 0.22$), maximum velocities (LW–MW: $p_B = 0.11$, LW–HW: $p_B = 0.04$, MW–HW: $p_B = 1$), minimum velocities ($p_A = 0.81$), nor in SPARC indices ($p_{KW} = 0.17$).

Elbow angles consistently started at the target angle θ_{des} and reached around $90°$, with average angle overshoots that were confined in the $1.12 - 1.65°$ range. Peaks of positive and negative elbow angular velocities ranged from $24.16 \pm 1.01\,°/\text{s}$ up to $33.60 \pm 1.53\,°/\text{s}$, and from $27.41 \pm 1.33\,°/\text{s}$ up to $29.05 \pm 0.87\,°/\text{s}$, respectively.

Finally, median SPARC indices ranged between -5.09 ± 0.10 and -5.75 ± 0.10, confirming with an additional metric, unaltered smoothness of the user kinematics.

VII. Discussion

The integration of collaborative and wearable robots represents a promising yet relatively unexplored avenue of research [25]. As industrial automation progresses toward seamless human–robot collaboration [1], [12], humans remain indispensable for their flexibility, dexterity, and cognitive abilities [3], [34]. Currently, collaborative robots and exoskeletons are typically developed and deployed in parallel for complementary purposes, with little to no interaction between them. When considered in isolation, both technologies exhibit inherent limitations: cobots cannot assist the user beyond their workspace and, in the absence of external sensing, rely on physical contact for interaction and lack user-specific adaptability. Conversely, for wearable robots, it remains challenging to modulate the provided assistance while manipulating external payloads. In this work, we demonstrate that integrating soft exoskeletons with collaborative robots can overcome these limitations. This work does not advocate the introduction of collaborative robots solely for payload estimation. Rather, it investigates the synergies achievable in industrial environments where collaborative and wearable robots already coexist, showing how bidirectional integration can enhance the capabilities of both systems beyond what each technology can achieve independently. In *WearaCob*, the cobot enables the exoskeleton to adapt its assistance according to the handled payload, providing effective support beyond the robot's workspace. Simultaneously, the exoskeleton's onboard sensing allows the cobot to adapt its behavior to the user's actions and anthropometric characteristics, thereby achieving a more natural and personalized form of physical collaboration.

A. Enhancing Adaptability, Efficiency, and Safety through User-Specific Handover

Communication between exoskeleton, vision, and cobot enabled user-specific handovers that adapt to approach di-

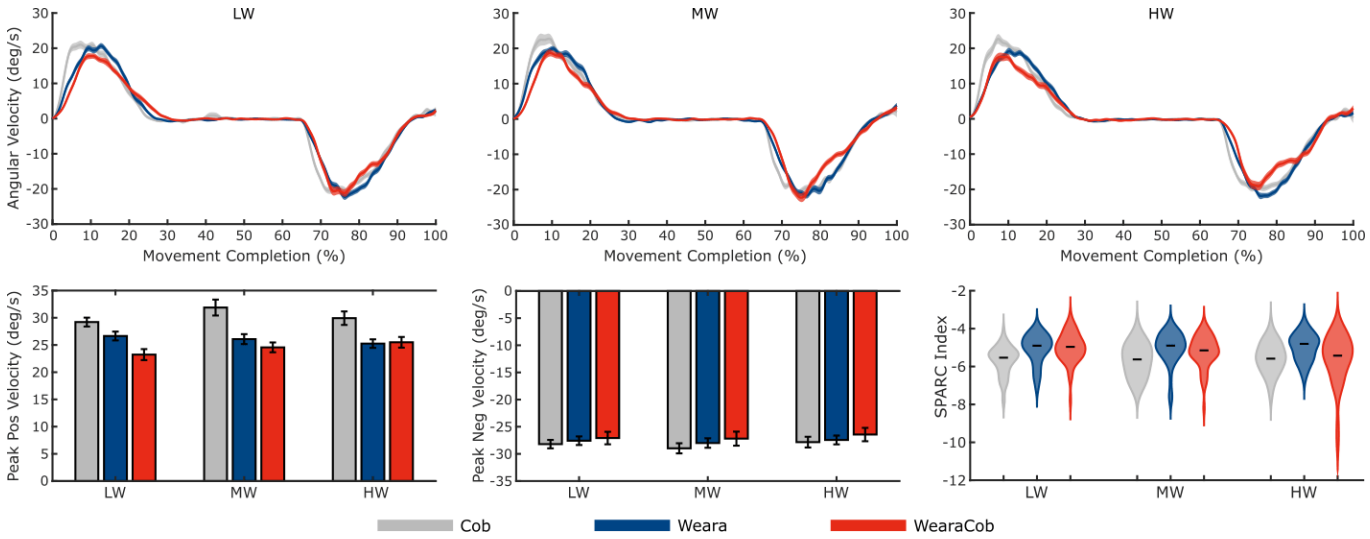

Fig. 6. Differential kinematics. This panel presents elbow angular velocity profiles recorded during the experimental task, bar plots of peak positive and negative velocities, and a violin plot of the SPARC index [30]. All data are reported as mean values with standard error across participants. Velocities are compared across three experimental conditions (*Cob*, *Weara*, *WearaCob*) and three external load levels (LW, MW, HW). Results indicate that neither the assistance conditions nor the external loads significantly affected velocity profiles or movement smoothness.

rection and anthropometry, improving efficiency and safety by placing the payload at an optimal pose for the operator and workcell. Empirically, elbow angle tracking at grasp showed high precision (mean error $0.46 \pm 1.00°$) despite height variability, while trunk inclination toward the payload remained minimal ($3.64 \pm 0.27°$), well below the $20°$ risk threshold associated with back injury [33], [35]. Despite the use of a fixed target elbow angle, the payload handover height varied across participants by approximately 9 cm due to differences in body height, confirming that the handover strategy adapts to user anthropometry. By maintaining the desired elbow angle and safe posture while accommodating arbitrary approach directions, *WearaCob* improves both interaction naturalness and operator safety. Future work will investigate personalized cobot–exoskeleton–human coordination, including multiple grasp configurations and a quantitative ergonomics evaluation.

B. Workload Reduction through Assistance Adaptation

A standalone soft exoskeleton (*Weara*) has difficulties in inferring object interaction or weight and thus typically compensates only for forearm mass [24]. EMG [21] and vision [22] face practical deployment hurdles (sensor placement, per-user calibration, perspiration/interaction artifacts, and closed containers). *WearaCob* overcomes these limitations by receiving the payload mass directly from the cobot, enabling object-agnostic, calibration-light assistance compatible with existing industrial deployments. Specifically, exoskeleton calibration relies only on user body mass M_u and height H_u, while camera–robot localization is performed exclusively on the robot side, via a one-time calibration of the ArUco markers with respect to the robot base. Experiments showed that biceps activation increased with load in *Cob*, was uniformly reduced but still load-dependent in *Weara*, and became small and load-invariant in *WearaCob*, confirming the benefit of the integration. The elbow torque analysis corroborated the conclusion. To probe unintended antagonistic effects [36], we examined triceps activity: like prior reports of antagonist engagement with exoskeletons [16], [37], activation appeared during lowering when extension is required; however, overall triceps activation did not differ significantly across conditions and was an order of magnitude smaller than the biceps reduction. Kinematic analysis showed no condition-dependent changes, indicating that the adaptive assistance preserved natural movement without compromising stability.

C. Context-Aware Control via Artificial Vision

Leveraging AI-enabled vision on embedded hardware expands situation-aware control for wearables [38], including terrain-adaptive assistance [39] and object-aware modulation [22]. In *WearaCob*, vision provides user localization for adaptive handover and detects payload release to deactivate unnecessary support. A short transient phase may occur between payload release and its detection by the vision module, during which the exoskeleton still provides load-related assistance. However, the release detection algorithm operates at $28\,\mathrm{fps}$, resulting in a very short delay that was not perceived as disturbing by the participants and did not affect task execution. A chest-mounted camera was chosen to maintain visual contact with the cobot, to reliably observe the hands during placement without external cameras, and to yield a self-contained system. Future work will explore alternative vision modalities to further enhance context-aware behavior.

VIII. Conclusion

We presented *WearaCob*, a novel system integrating exoskeletons, computer vision, and collaborative robots. Our experimental findings validated the system's ability to dynamically adapt the exoskeleton's assistance, resulting in a substantial reduction in muscular effort.

Notably, our approach ensures that the level of muscular effort remains constant despite variations in external loads, without significantly altering user kinematics. Finally, the system demonstrated the ability to tailor the handover process by dynamically adapting the cobot's behavior based on the operator's localization and anthropometric parameters.

Overall, these findings support our initial hypothesis and underscore the potential of *WearaCob* in improving efficiency, safety, and user-specific adaptability of human-robot collaboration, paving the way for a new paradigm in assistive industrial automation.

REFERENCES

[1] F. Sherwani, M. M. Asad, and B. S. K. K. Ibrahim, "Collaborative robots and industrial revolution 4.0 (ir 4.0)," in *2020 International Conference on Emerging Trends in Smart Technologies (ICETST)*, pp. 1–5, IEEE, 2020.

[2] M. Kostrzewski, P. Varjan, and J. Gnap, *Solutions Dedicated to Internal Logistics 4.0*, pp. 243–262. Cham: Springer International Publishing, 2020.

[3] V. Villani, F. Pini, F. Leali, and C. Secchi, "Survey on human–robot collaboration in industrial settings: Safety, intuitive interfaces and applications," *Mechatronics*, vol. 55, pp. 248–266, 2018.

[4] B. D. Argall and A. G. Billard, "A survey of tactile human–robot interactions," *Robotics and autonomous systems*, vol. 58, no. 10, pp. 1159–1176, 2010.

[5] A. De Santis, B. Siciliano, A. De Luca, and A. Bicchi, "An atlas of physical human–robot interaction," *Mechanism and Machine Theory*, vol. 43, no. 3, pp. 253–270, 2008.

[6] G. Michalos, S. Makris, J. Spiliotopoulos, I. Misios, P. Tsarouchi, and G. Chryssolouris, "Robo-partner: Seamless human-robot cooperation for intelligent, flexible and safe operations in the assembly factories of the future," *Procedia CIRP*, vol. 23, pp. 71–76, 2014. 5th CATS 2014 - CIRP Conference on Assembly Technologies and Systems.

[7] T. B. Sheridan, "Human–robot interaction: Status and challenges," *Human Factors*, vol. 58, no. 4, pp. 525–532, 2016. PMID: 27098262.

[8] A. Ajoudani, A. M. Zanchettin, S. Ivaldi, A. Albu-Schäffer, K. Kosuge, and O. Khatib, "Progress and prospects of the human–robot collaboration," *Autonomous robots*, vol. 42, pp. 957–975, 2018.

[9] M. Xiloyannis, D. Chiaradia, A. Frisoli, and L. Masia, "Physiological and kinematic effects of a soft exosuit on arm movements," *Journal of NeuroEngineering and Rehabilitation*, vol. 16, no. 1, p. 29, 2019.

[10] M. Rüßmann, M. Lorenz, P. Gerbert, M. Waldner, J. Justus, P. Engel, and M. Harnisch, "Industry 4.0: The future of productivity and growth in manufacturing industries," *Boston consulting group*, vol. 9, no. 1, pp. 54–89, 2015.

[11] S. Haddadin, A. De Luca, and A. Albu-Schäffer, "Robot collisions: A survey on detection, isolation, and identification," *IEEE Transactions on Robotics*, vol. 33, no. 6, pp. 1292–1312, 2017.

[12] E. Matheson, R. Minto, E. G. Zampieri, M. Faccio, and G. Rosati, "Human–robot collaboration in manufacturing applications: a review," *Robotics*, vol. 8, no. 4, p. 100, 2019.

[13] L. van der Spaa, M. Gienger, T. Bates, and J. Kober, "Predicting and optimizing ergonomics in physical human-robot cooperation tasks," in *2020 IEEE International Conference on Robotics and Automation (ICRA)*, pp. 1799–1805, IEEE, 2020.

[14] W. Kim, J. Lee, L. Peternel, N. Tsagarakis, and A. Ajoudani, "Anticipatory robot assistance for the prevention of human static joint overloading in human–robot collaboration," *IEEE robotics and automation letters*, vol. 3, no. 1, pp. 68–75, 2017.

[15] W. Kim, L. Peternel, M. Lorenzini, J. Babič, and A. Ajoudani, "A human-robot collaboration framework for improving ergonomics during dexterous operation of power tools," *Robotics and Computer-Integrated Manufacturing*, vol. 68, p. 102084, 2021.

[16] S. Crea, P. Beckerle, M. De Looze, K. De Pauw, L. Grazi, T. Kermavnar, J. Masood, L. W. O'Sullivan, I. Pacifico, C. Rodriguez-Guerrero, *et al.*, "Occupational exoskeletons: A roadmap toward large-scale adoption. methodology and challenges of bringing exoskeletons to workplaces," *Wearable Technologies*, vol. 2, p. e11, 2021.

[17] R. Bogue, "Robotic exoskeletons: a review of recent progress," *Industrial Robot: An International Journal*, vol. 42, no. 1, pp. 5–10, 2015.

[18] M. P. De Looze, F. Krause, and L. W. O'Sullivan, "The potential and acceptance of exoskeletons in industry," in *Wearable Robotics: Challenges and Trends: Proceedings of the 2nd International Symposium on Wearable Robotics, WeRob2016, October 18-21, 2016, Segovia, Spain*, pp. 195–199, Springer, 2016.

[19] M. Xiloyannis, R. Alicea, A.-M. Georgarakis, F. L. Haufe, P. Wolf, L. Masia, and R. Riener, "Soft robotic suits: State of the art, core technologies, and open challenges," *IEEE Transactions on Robotics*, vol. 38, no. 3, pp. 1343–1362, 2021.

[20] E. Mobedi, S. Hjorth, W. Kim, E. De Momi, N. G. Tsagarakis, and A. Ajoudani, "A power-aware control strategy for an elbow effort-compensation device," *IEEE Robotics and Automation Letters*, vol. 8, no. 7, pp. 4330–4337, 2023.

[21] N. Lotti, M. Xiloyannis, G. Durandau, E. Galofaro, V. Sanguineti, L. Masia, and M. Sartori, "Adaptive model-based myoelectric control for a soft wearable arm exosuit: A new generation of wearable robot control," *IEEE Robotics & Automation Magazine*, vol. 27, no. 1, pp. 43–53, 2020.

[22] F. Missiroli, P. Mazzoni, N. Lotti, E. Tricomi, F. Braghin, L. Roveda, and L. Masia, "Integrating computer vision in exosuits for adaptive support and reduced muscle strain in industrial environments," *IEEE Robotics and Automation Letters*, vol. 9, no. 1, pp. 859–866, 2024.

[23] H. van der Kooij, E. H. van Asseldonk, M. Sartori, C. Basla, A. Esser, and R. Riener, "Ai in therapeutic and assistive exoskeletons and exosuits: Influences on performance and autonomy," *Science Robotics*, vol. 10, no. 104, p. eadt7329, 2025.

[24] N. Lotti, M. Xiloyannis, F. Missiroli, C. Bokranz, D. Chiaradia, A. Frisoli, R. Riener, and L. Masia, "Myoelectric or force control? a comparative study on a soft arm exosuit," *IEEE Transactions on Robotics*, vol. 38, no. 3, pp. 1363–1379, 2022.

[25] E. Mobedi, G. Solak, and A. Ajoudani, "A framework for adaptive load redistribution in human-exoskeleton-cobot systems," *IEEE Robotics and Automation Letters*, 2025.

[26] S. Haddadin, S. Parusel, L. Johannsmeier, S. Golz, S. Gabl, F. Walch, M. Sabaghian, C. Jähne, L. Hausperger, and S. Haddadin, "The franka emika robot: A reference platform for robotics research and education," *IEEE Robotics & Automation Magazine*, vol. 29, no. 2, pp. 46–64, 2022.

[27] M. Kalaitzakis, B. Cain, S. Carroll, A. Ambrosi, C. Whitehead, and N. Vitzilaios, "Fiducial markers for pose estimation: Overview, applications and experimental comparison of the artag, apriltag, aruco and stag markers," *Journal of Intelligent & Robotic Systems*, vol. 101, pp. 1–26, 2021.

[28] R. Drillis and R. Contini, *Body Segment Parameters*. New York: New York University, School of Engineering and Science, Research Division, 1966.

[29] M. Dempster and R. C. Nelson, *Biomechanics of Sport*. Philadelphia: Lea and Febiger, 1973.

[30] S. Balasubramanian, A. Melendez-Calderon, A. Roby-Brami, and E. Burdet, "On the analysis of movement smoothness," *Journal of NeuroEngineering and Rehabilitation*, vol. 12, no. 1, pp. 1–11, 2015.

[31] Google, "Mediapipe: Cross-platform, customizable ml solutions for live and streaming media," 2023. Available at https://mediapipe.dev.

[32] S. Project, "Seniam guidelines: Surface electromyography for the non-invasive assessment of muscles." https://www.seniam.org, 2000. Accessed: 2023-02-07.

[33] W. S. Marras, K. G. Davis, B. C. Kirking, and S. A. Murphy, "A longitudinal study of low back pain and operator posture in the automotive assembly industry," *Ergonomics*, vol. 36, no. 4, pp. 319–328, 1993.

[34] J. Krüger, T. K. Lien, and A. Verl, "Cooperation of human and machines in assembly lines," *CIRP annals*, vol. 58, no. 2, pp. 628–646, 2009.

[35] T. R. Waters, V. Putz-Anderson, A. Garg, and L. J. Fine, "Applications of the revised niosh lifting equation to manual lifting tasks," *Ergonomics*, vol. 36, no. 7, pp. 773–789, 1993.

[36] Y. M. Zhou, C. J. Hohimer, H. T. Young, C. M. McCann, D. Pont-Esteban, U. S. Civici, Y. Jin, P. Murphy, D. Wagner, T. Cole, *et al.*, "A portable inflatable soft wearable robot to assist the shoulder during industrial work," *Science Robotics*, vol. 9, no. 91, p. eadi2377, 2024.

[37] A. De Vries and M. De Looze, "The effect of arm support exoskeletons in realistic work activities: a review study," *J. Ergon*, vol. 9, no. 4, pp. 1–9, 2019.

[38] D. Kim, B. B. Kang, K. B. Kim, H. Choi, J. Ha, K.-J. Cho, and S. Jo, "Eyes are faster than hands: A soft wearable robot learns user intention from the egocentric view," *Science Robotics*, vol. 4, no. 26, p. eaav2949, 2019.

[39] E. Tricomi, G. Piccolo, F. Russo, X. Zhang, F. Missiroli, S. Ferrari, L. Gionfrida, F. Ficuciello, M. Xiloyannis, and L. Masia, "Leveraging geometric modeling-based computer vision for context aware control in a hip exosuit," *IEEE Transactions on Robotics*, vol. 41, pp. 3462–3479, 2025.